GA–A26981

PROGRESS IN STEADY-STATE SCENARIO DEVELOPMENT IN THE DIII-D TOKAMAK

by

T.C. LUCE, J.R. FERRON, C.T. HOLCOMB, F. TURCO,
P.A. POLITZER, and T.W. PETRIE

JANUARY 2011

GENERAL ATOMICS

DISCLAIMER

GA–A26981

PROGRESS IN STEADY-STATE SCENARIO DEVELOPMENT IN THE DIII-D TOKAMAK

by
T.C. LUCE, J.R. FERRON, C.T. HOLCOMB[1], F. TURCO[2],
P.A. POLITZER, and T.W. PETRIE

This is a preprint of a paper to be presented at the 6th IAEA Technical Meeting on Steady-State Operation of Magnetic Fusion Devices, in Vienna, Austria, December 6–10, 2010 and to be published in the *Proceedings*.

[1]Lawrence Livermore National Laboratory, Livermore, California
[2]Oak Ridge Institute for Science Education, Oak Ridge, Tennessee

Work supported by
the U.S. Department of Energy
under DE-FC02-04ER54698, DE-AC52-07NA27344,
and DE-AC05-06ER23100

GENERAL ATOMICS PROJECT 30200
JANUARY 2011

GENERAL ATOMICS

1. Introduction

Since the last Technical Meeting on Steady State Operation (Daejeon, 2007), progress has been made in experiments on the DIII-D tokamak to develop integrated scenarios for steady state operation. A focal point of the recent experiments is the optimization of the magnetic configuration. Two specific optimizations of the magnetic configuration will be discussed here — the shape of the plasma boundary and the internal magnetic structure as measured by the *q* profile. These optimization studies of tokamak plasmas point to specific implications for the design of a power plant.

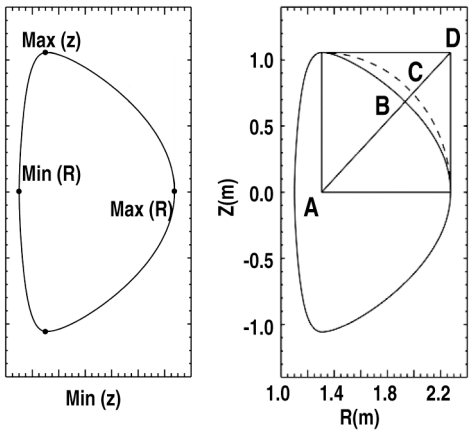

Fig. 1. (a) Plasma cross-section showing points for definition of the following dimen-sionless parameters: $R_{geo} \equiv [max(R) + min(R)]/2$, $a \equiv [max(R) - min(R)]/2$, $A \equiv R_{geo}/a$, $\kappa \equiv [max(Z) - min(Z)]/a$, $\delta_u \equiv R_{geo} - R[max(Z)]/a$, $\delta_l \equiv R_{geo} - R[min(Z)]/a$, where subscripts u and l corre-spond to upper and lower, respectively; (b) Plasma cross-section showing points for definition of squareness $\zeta_{ou} \equiv (AB-AC)/CD$, where subscript ou stands for "outer upper". The squareness values in the other 3 quadrants (ζ_{ol}, ζ_{iu}, ζ_{il}) are defined in an analogous fashion.

2. Influence of the Plasma Boundary Shape

The plasma boundary shape is usually characterized by a few dimensionless geometric parameters — aspect ratio (A), elongation (κ), and triangularity (δ). [See Fig. 1(a) for definitions of these quantities.] In tokamak power plant design, there is little freedom of choice in these parameters. The value of A is usually set by the constraint of the desired flux capacity of the central solenoid and the thickness of the shielding required for a specified fusion power output. Similarly, δ is typically maximized within constraints of heat flux to the divertor and engineering of the poloidal field coils with respect to shielding. Stabilization of the plasma to axisymmetric perturbations (*n*=0, where *n* is the toroidal mode number) sets an upper limit on κ, which is usually maximized. However, there remains a relatively unexplored geometric parameter known as squareness (ζ) that has significant impact on the plasma stability and energy confinement. [See Fig. 1(b) for definition of this quantity.] The standard scalar metric for stability [$\beta_N \equiv \beta/(I/aB)$] has shaping implicitly included, while the standard scalar metrics for confinement ($H \equiv \tau/\tau_{scaling}$) typically have the effect of A and κ explicitly included, but not the higher order shaping parameters (δ, ζ).

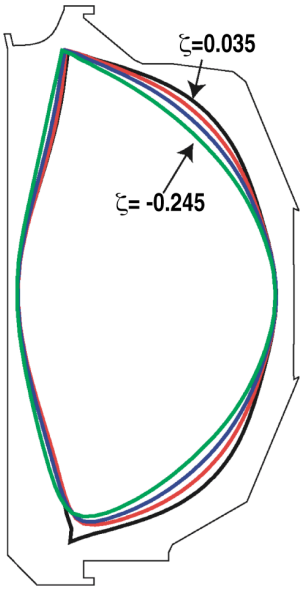

Fig. 2. Cross-sections of DIII-D plasmas showing the variation in ζ in the experiments discussed in the text. The outer solid line shows the location of the plasma-facing components.

Experiments on DIII-D explored variations in ζ on the outside boundary of the plasma (ζ_{ou} and ζ_{ol}) with relatively fixed κ and δ (Fig. 2) [1]. A slight imbalance in the plasma toward the upper divertor was employed for reasons discussed later, but the ζ changes were nearly up-down symmetric. One of the motivations for exploring the changes in ζ experimentally was the observation that the ideal-MHD stability to *n*=1 perturbations (with and without a conducting wall)

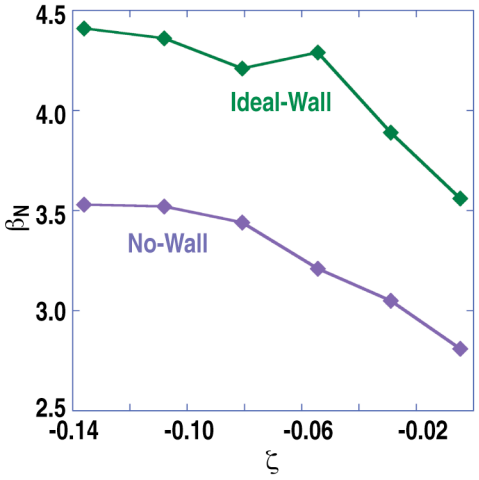

Fig. 3. Calculated ideal-MHD n=1 stability limits without (blue) and with (green) an ideal conducting wall as a function of ζ.

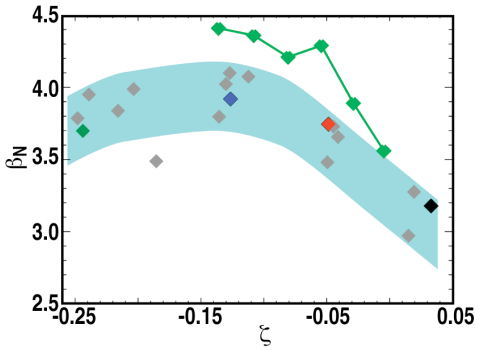

Fig. 4. Variation of experimentally achieved β_N (light blue band) with the predicted ideal-MHD n=1 limits with an ideal conducting wall (green line) as a function of ζ. The colored diamonds correspond to the shapes of the same color in Fig. 2

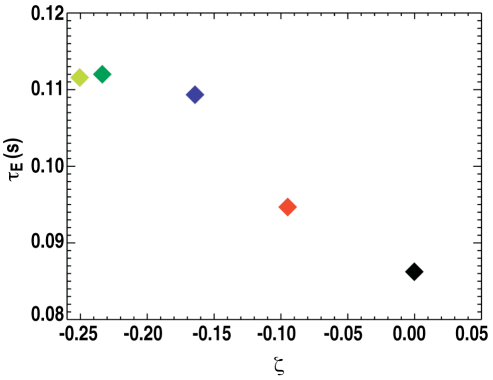

Fig. 5. Variation of the experiment global confinement time with ζ. The colors correspond to the shapes shown in Fig. 2.

increased significantly as ζ decreased (Fig. 3) [2]. The fact that the no-wall limit improved and the ideal-wall improved despite increasing the average distance to the wall on the outboard side indicated that this was an effect intrinsic to the change in shape. Experiments (Fig. 4) showed that the effective pressure limit in quasi-stationary plasmas followed the predicted trend from ideal-MHD. The experimental scan extended beyond the range in ζ of the theoretical predictions and found a weak optimum between ζ = -0.15 and ζ = -0.1. Surprisingly, the global energy confinement also had a strong increase as ζ decreased (Fig. 5). The range in ζ was not sufficient to find a clear optimum for τ_E. The change in ζ resulted in both an increase in the pedestal pressure and pressure gradient (Fig. 6), which agreed with stability calculations using peeling-ballooning mode theory (Fig. 6). However, the fractional variation in the total plasma stored energy was greater than the fractional variation in the pedestal, indicating a more global effect of the shape change. This, along with the fact that the confinement improved despite a decrease in volume, indicates a significant intrinsic effect of this higher-order change in shape on the stability of both the pedestal and the turbulence that governs energy transport in the outer part of the plasma.

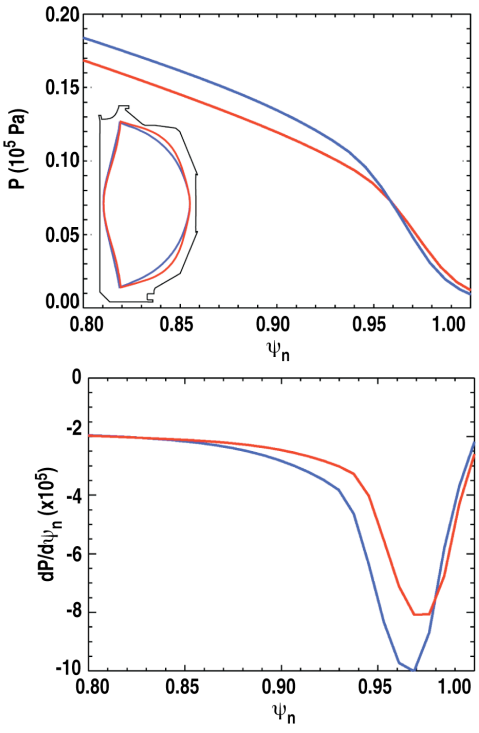

Fig. 6. Plasma pressure (a) and pressure gradient (b) as a function of normalized poloidal flux (ψ_N) for the two shapes shown in the inset.

The implication for tokamak power plant design is to locate the outer poloidal field coils to allow some variation in the plasma boundary in order to optimize with respect to this shape parameter. This would appear to be a rather modest constraint on design, with potentially large impact on fusion gain

through the increases in pressure limit and energy confinement.

In addition to core plasma performance, the plasma shape affects significantly the performance of the divertor. A key strategic decision facing the tokamak power plant designer is whether to have one or two divertors (single-null plasma or double-null plasma). The DIII-D steady-state experiments have been carried out in plasmas close to double-null, because the achievable β_N is higher for a given A, κ, and δ, and the β is higher for fixed β_N and q_{95} due to the increased plasma current. However, it was found that the divertor conditions optimize with a slight imbalance, measured by the radial distance at the outboard midplane between magnetic field lines that connect to the upper and lower divertor nulls (dR_{sep}) [1]. (By convention, dR_{sep} is positive when the upper divertor is connected to the inner field line and negative when the lower null is connected.) For the standard direction of toroidal magnetic field in DIII-D, the ion ∇B drift is downward. As dR_{sep} is varied, the plasma density is strongly reduced only for $dR_{sep} > 0$, i.e., when the upper divertor is the active divertor (Fig. 7). Only about 5 mm of separation is needed to see a strong effect, although the effect is stronger for larger dR_{sep}. The global energy confinement does not show a corresponding change, indicated this is primarily a divertor effect and less due to any change in confinement in the core plasma. Modeling indicates that the explanation for this asymmetry lies in the flow patterns in the scrape-off layer (SOL) and divertor largely generated by $E \times B$ drifts (Fig. 8) [3]. In particular, both experiment and modeling show that when the $E \times B$ drift in the private flux region of the divertor is toward the outer leg, the recycling light is much stronger there, and the pump can capture more effectively the recycling particles. When the $E \times B$ drift is in the opposite direction, the resulting higher density and lower electron temperature along the inner divertor leg provides strong rrecycling and a significant fueling source to the main plasma [4]. If the inner divertor leg continues to cool and eventually detaches, the relatively cold plasma can extend toward the inboard midplane, allowing neutrals more direct access to the core plasma.

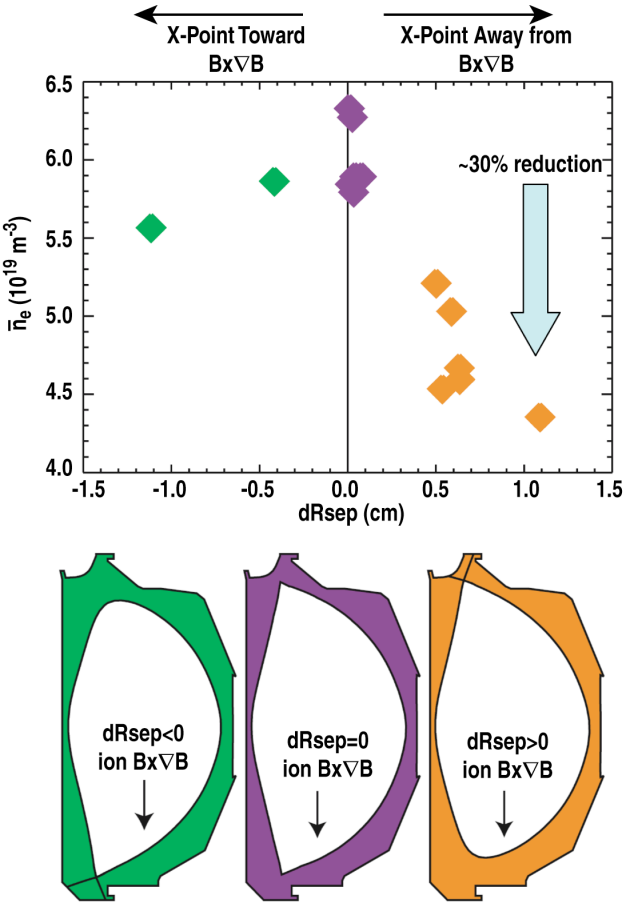

Fig. 7. (a) Line-averaged density (n) vs dR_{sep}. (b) Plasma shapes corresponding to the variation in dR_{sep}.

While density reduction is important for DIII-D scenarios to maximize the noninductive current driven, the issue for a power plant is primarily control of both the helium ash and the extrinsic impurities used for steady-state heat flux control through a radiative divertor. It appears favorable from this point of view to run either a single-null divertor with ion ∇B drift out of the divertor (opposite of the conventional direction) or a double-null divertor slightly unbalanced in that direction, as in the DIII-D experiments. This has the consequence of raising the threshold

power for reaching H-mode operation, which is already a challenging issue for next-generation tokamaks like ITER. However, this effect may be reduced at low rotation.

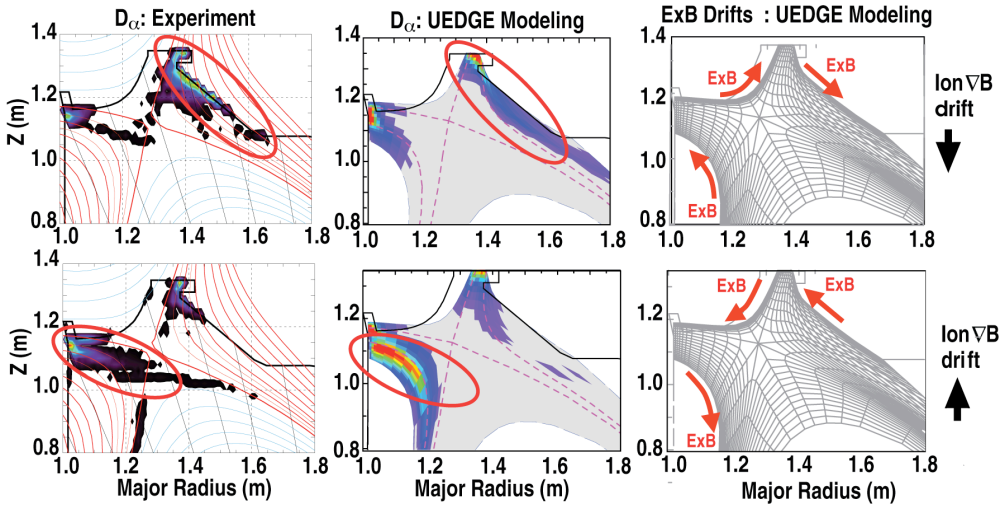

Fig. 8. Experimental D_α measurements (left column), calculated D_α emission (central column), and schematic showing ExB flow patterns (right column) for plasmas with the ion ∇B drift out of (upper row) and into (lower row) the upper divertor.

3. Importance of the *q* Profile

Steady-state tokamak operation at high-energy gain requires the majority of the plasma current to be sustained by the bootstrap current. The local bootstrap current density is proportional to q, to the pressure, and to the individual profile scale lengths (electron and ion density and temperature) [5]. However, energy and particle transport depends on both q and magnetic shear ($\hat{s} \equiv d(\ln q)/dr$) [6]. Therefore, the bootstrap current depends on q both directly and in a more complicated way through the kinetic scale lengths. Since the q profile is dominated by the bootstrap current, there is a significant feedback loop that must evolve self-consistently on the confinement and resistive time scales.

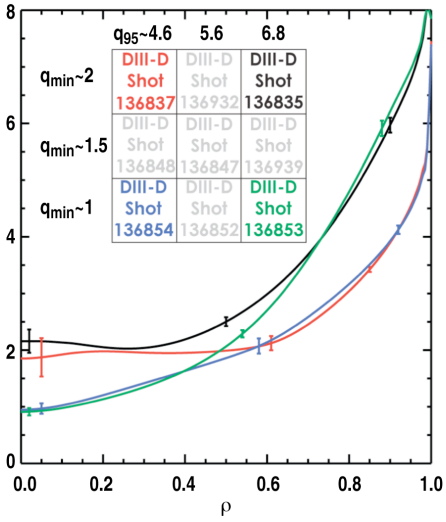

Fig. 9. Radial profile of q for the 4 extremes of the q_{min}, q_{95} scan discussed in the text. The legend shows the color code for the profiles shown. The radial coordinate is the square root of the normalized toroidal flux.

In the absence of a transport model with validation of the dependence on q and $\hat{s}$, DIII-D experiments were undertaken to find the self-consistent response to variations in the current profile [7]. Variations in $q_{\min}$ (1, 1.5, 2) and q_{95} (4.6, 5.6, 6.8) were studied; the q profiles for the four extremes are shown in Fig. 9, for cases with fixed β_N in order to isolate the transport effects. Cases at the maximum attainable β_N were also studied to include the effects of the pressure limits on the bootstrap fraction. The resulting electron and ion temperature profiles are shown in Fig. 10. The density profiles show a similar, but less dramatic effect. The general observation is that increasing $q_{\min}$ leads to a broadening of the profiles. The corresponding reduction in the kinetic gradients (Fig. 11) therefore offsets some of the anticipated gain in

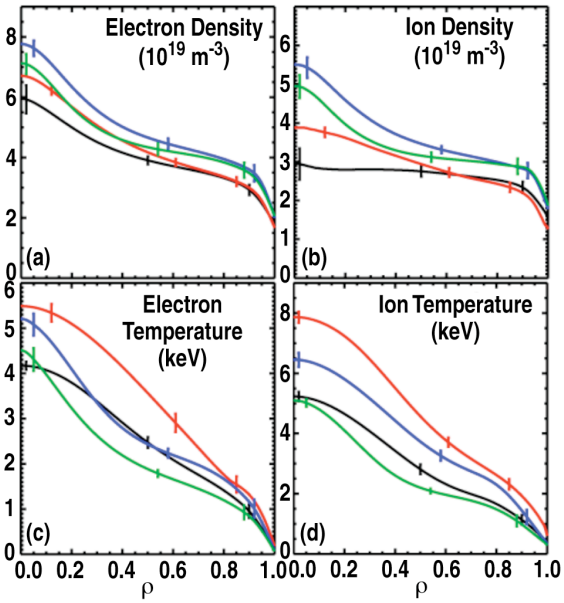

Fig. 10. Radial profiles of the (a) electron and (b) ion temperature. The colors correspond to the legend in Fig. 9

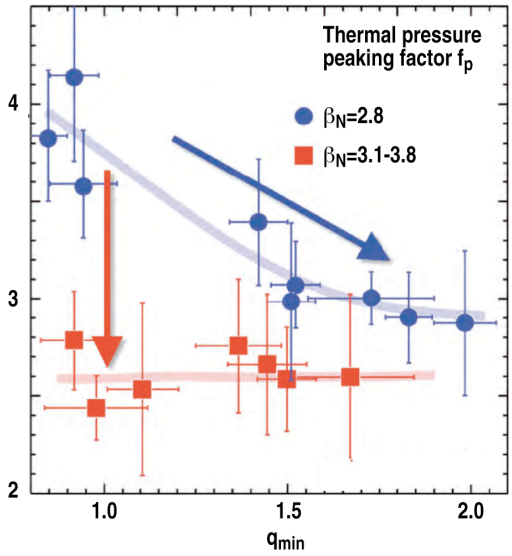

Fig. 11. Thermal pressure peaking factor vs q_{min} for a scan at constant β_N (blue) and maximum attained β_N under quasi-stationary conditions (red).

bootstrap current commonly associated with an increase in $q_{\min}$. The profiles also broaden with increased β_N (Fig. 11), again lessening the anticipated gain in bootstrap current with increased pressure. While the calculated bootstrap current fraction (f_{BS}) is linear with β_N and q_{95} (Fig. 12), there is an offset that depends on β_N. A functional form for the bootstrap current fraction motivated by the theoretical formula fits the experimental data much better than the standard form $f_{BS} \propto \beta_N q_{95}$. That form (Fig. 13) is proportional to β_N and has separate terms proportional to the value of q in the core and at the edge with power law dependencies on the pressure peaking.

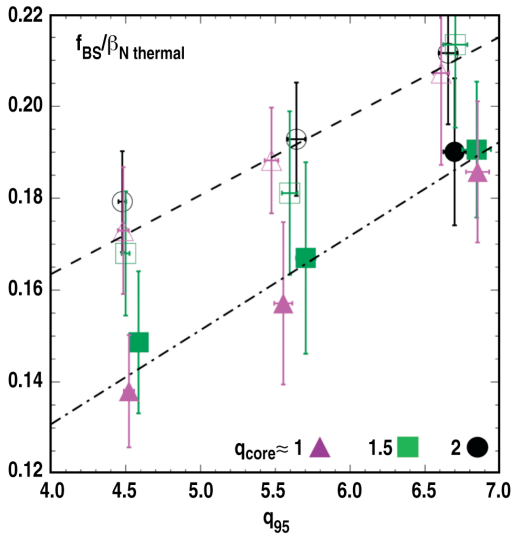

Fig. 12. Bootstrap current fraction normalized to β_N as a function of q_{95}. The open symbols are from a scan at constant β_N and the closed symbols are for a scan at maximum attained β_N under quasi-stationary conditions.

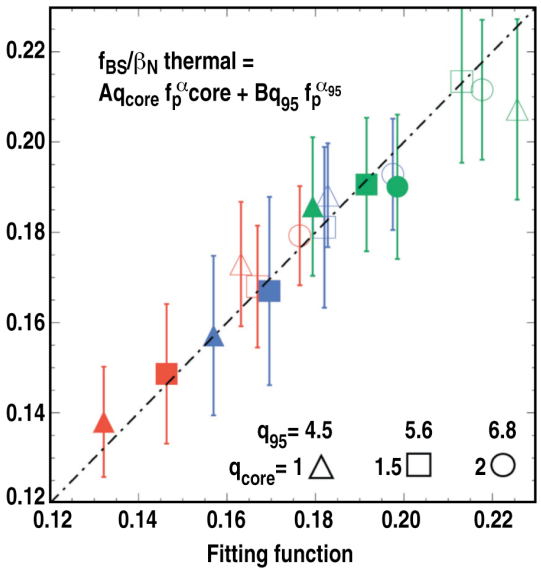

Fig. 13. Comparison of the experimental values of bootstrap current fraction normalized to β_N to a fitting function motivated by the standard theoretical form.

Another emerging issue for steady-state tokamaks is avoidance of tearing instabilities, both in the formation and steady-state phases. As illustrated above, ideal-MHD stability calculations can guide experiments and design; however, the corresponding predictive capabilities for avoiding tearing modes and design optimization do not exist. Again, in the absence of a validated model, experiments were undertaken to see how modification of the current profile could avoid tearing modes. In DIII-D, the flexibility of electron cyclotron current drive (ECCD) was used to probe tearing stability. It was observed that broad ECCD deposition was more favorable for tearing stability than localized deposition (Fig. 14) [8]. The effect of ECCD was inferred to be causal with respect to stability by a temporal correlation of stability with the presence of the ECCD (Fig. 15). After the broad deposition ECCD was removed the n=1 tearing mode appeared on a time scale consistent with decay of the back emf that results from the loss of the ECCD. These two effects indicate that the stabilization is not due to direct interaction of the local ECCD at a low-order rational surface, but due to a more global effect through modification of the current profile. Subsequent experiments probing a larger variation in ECCD location and deposition profile width were less definitive than the early experiments shown here. These results can be reconciled by the hypothesis that the classical tearing parameter Δ' is strongly affected by proximity to the ideal-MHD limit to external modes, in analogy to previous analysis for internal modes [9]. Preliminary calculations support this hypothesis and will reported in a future publication [10].

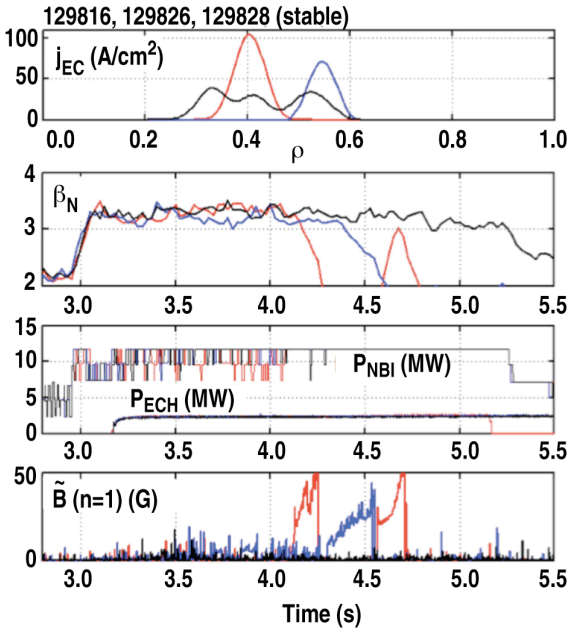

Fig. 14. Time histories of β_N, neutral beam and electron cyclotron power, n=1 magnetic fluctuation amplitude for 3 plasmas with the ECCD deposition profile shown in the top box.

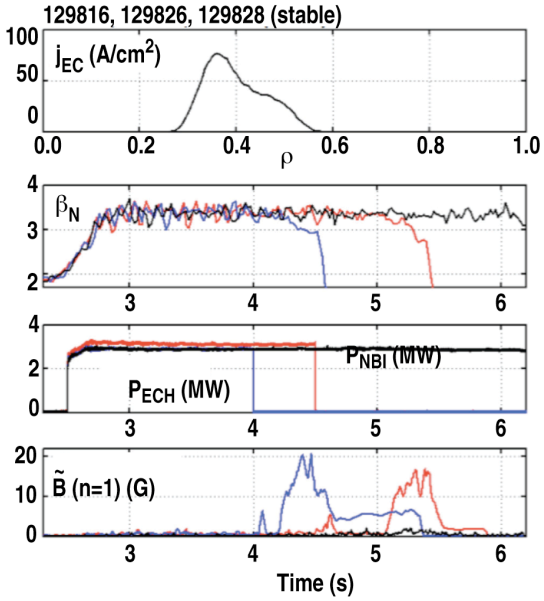

Fig. 15. Time histories of β_N, electron cyclotron power, n=1 magnetic fluctuation amplitude for 3 plasmas with the ECCD deposition profile shown in the top box. The timing of the end of the electron cyclotron power is intentional varied in the 3 cases.

There are two key implications of the sensitivity to the current profile for steady-state tokamak design. First is that some capability to bias the steady-state current profile will be needed. Even if 100% bootstrap current can be achieved, it is not obvious that the resulting pressure and current profiles will be stable both to ideal-MHD and tearing modes. A noninductive current drive system that can drive current with arbitrary radial deposition appears to be necessary to tailor the total current profile to ensure

stability. (The pressure profile modification will be relatively small at high fusion gain.) A similar system is also likely required to ensure producible and stable access to the desired operating point. Second, the goal of eliminating or at least reducing the central solenoid for steady-state tokamaks is attractive, but the central solenoid, combined with the ability to change the conductivity profile, is the only known method to generate a wide variety of initial current profiles to initiate the burn phase of a steady-state tokamak. At present, ECCD is the only non-inductive current drive system that exhibits the flexibility that may be required.

4. Integrated Scenario Demonstration

The optimization studies above have been combined to yield an integrated solution in DIII-D for durations approaching a resistive time (Fig. 16) [1]. Reconstruction of the magnetic equilibrium shows a relatively broad current profile with substantial current density in the edge pedestal (Fig. 17). From the time history of the reconstructions, the inferred inductive current density is small and not quite in equilibrium (Fig. 17), consistent with the duration being less than a resistive time. Modeling of the non-inductive current sources is in good agreement the equilibrium reconstruction (Fig. 18). The pedestal current density is consistent with the expected bootstrap current there. The ECCD is used in a broad deposition to provide tearing stability. The duration of the high performance phase is limited by the energy limits of the neutral beam injection system and not by instability.

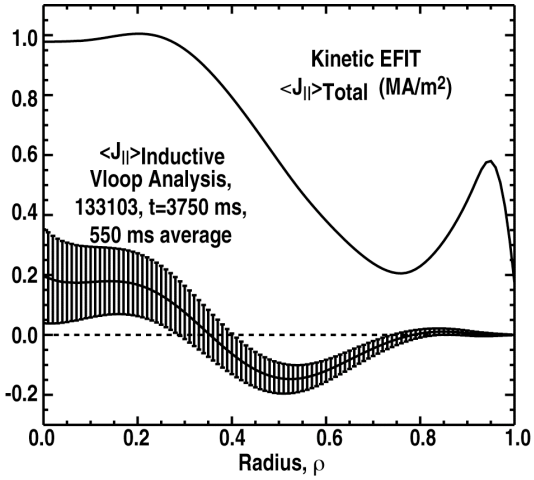

Fig. 17. Radial profiles of the total and inductive current densities.

Upgrades of the heating and current drive systems in DIII-D will allow extension and further optimization of this scenario. The energy capacity of the neutral beams will be enhanced by modification of the sources and improvement of the internal ion dumps. The goal is 10 s operation at nominal full power (15 MW of co-

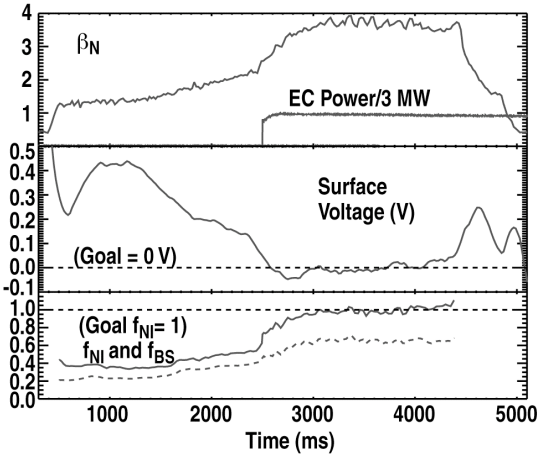

Fig. 16. Time histories of β_N, electron cyclotron power (top box), surface voltage (middle box), and noninductive and bootstrap current fractions (bottom box) for an integrated steady-state scenario plasma.

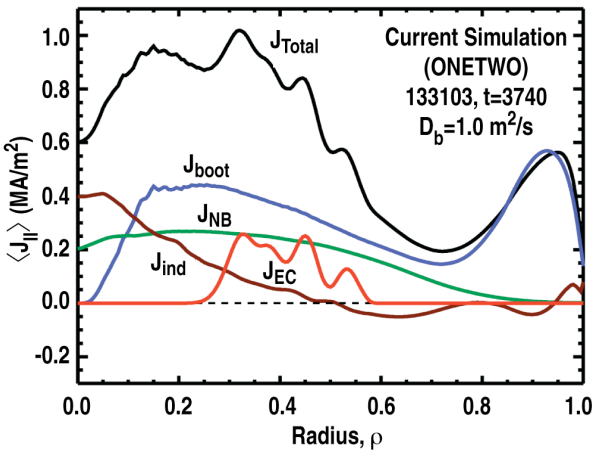

Fig. 18. Radial profiles of the calculated total (black), bootstrap (blue), neutral beam (green), electron cyclotron (red), and inductive (purple) current densities.

injection). One of the beamlines is being modified to be tilted vertically to allow off-axis neutral beam current drive (NBCD). When all of co-injection neutral beams are used to reach high β_N, the central NBCD precludes operation at $q_{min}>2$, where ideal-MHD stability calculations indicate the wall-stabilized pressure limit should be in the range thought necessary for economic steady-state tokamak operation ($\beta_N=5$). Increases in the EC system power in the near-term (from 5 MW to 8.5 MW at the source) will also increase the off-axis current drive capability. The combination of these two upgrades should provide substantial flexibility to explore different magnetic configurations to optimize the plasma for steady-state operation.

This work was supported in part by the US Department of Energy under DE-FC02-04ER54698, DE-AC52-07NA27344, and DE-AC05-06OR23100.

References

[1] C.T. Holcomb, *et al.,* Phys. Plasmas **16**, 056116 (2009).
[2] C.E. Kessel, *et al.,* in *Proc. of the 30th European Conf. on Controlled Fusion and Plasma Physics*, St. Petersburg, 2003, edited by R. Koch and S. Lebedev, European Physical Society, Geneva, 2003, ECA Vol. 27, Paper 4.044.
[3] T.W. Petrie, *et al.,* Nucl. Fusion **49**, 065013 (2009).
[4] M. Groth, et al., J. Nucl. Mater. **337-339**, 425 (2005).
[5] O. Sauter, *et al.,* Phys. Plasmas **6**, 2834 (1999).
[6] R.E. Waltz, *et al.,* Phys. Plasmas **2**, 2408 (1995).
[7] J.R. Ferron, *et al.,* "Optimization of the safety factor profile for high noninductive current fraction discharges in DIII-D," submitted to Nucl. Fusion (2010).
[8] T.C. Luce, "Role of ECH and ECCD in High-Performance Steady-State Scenarios," in *Proc. of the 16th Joint Workshop on Electron Cyclotron Emission and EC Resonance Heating, Sanya, China* (2010).
[9] D.P. Brennan, *et al.,* Phys. Plasmas **10**, 1643 (2003).
[10] F. Turco, *et al,* Bull Am. Phys. Soc. **55**, 61 (2010).